Journal of Alloys and Compounds 509 (2011) 3319–3325

Contents lists available at ScienceDirect

Journal of Alloys and Compounds

journal homepage: www.elsevier.com/locate/jallcom

Microstructure, kinetic analysis and hardness of Sn–Ag–Cu–1 wt% nano-ZrO_2 composite solder on OSP-Cu pads

Asit Kumar Gain[a], Tama Fouzder[a], Y.C. Chan[a,*], Winco K.C. Yung[b]

[a] Department of Electronic Engineering, City University of Hong Kong, Tat Chee Avenue, Kowloon Tong, Hong Kong
[b] Department of Industrial and Systems Engineering, The Hong Kong Polytechnic University, Hung Hom, Kowloon, Hong Kong

ARTICLE INFO

Article history:
Received 27 September 2010
Received in revised form 5 December 2010
Accepted 7 December 2010
Available online 14 December 2010

Keywords:
Nano doping
Microstructure
Kinetics analysis
Hardness

ABSTRACT

Nano-sized, nonreacting, noncoarsening ZrO_2 particle-reinforced Sn–Ag–Cu composite solders were prepared by mechanically dispersing ZrO_2 nano-particles into Sn–Ag–Cu solder and the interfacial morphology between the solder and organic solderability preservative (OSP)-Cu pads were characterized metallographically. At their interfaces, island-shaped Cu_6Sn_5 and Cu_3Sn intermetallic compound (IMC) layers were found in solder joints with and without the ZrO_2 particles and the IMC layer thickness was substantially increased with reaction time and temperature. In the solder ball region, needle-shaped Ag_3Sn and spherically-shaped Cu_6Sn_5 IMC particles were found to be uniformly distributed in the β–Sn matrix. However, after the addition of ZrO_2 nano-particles, Ag_3Sn and Cu_6Sn_5 IMC particles appeared with a fine microstructure and retarded the growth rate of the IMC layers at their interfaces. From a kinetic analysis, the calculated activation energies for the total (Cu_6Sn_5 + Cu_3Sn) IMC layers for Sn–Ag–Cu and Sn–Ag–Cu–1 wt% ZrO_2 composite solder joints on OSP-Cu pads were about 53.2 and 59.5 kJ/mol, respectively. In addition, solder joints containing ZrO_2 nano-particles displayed higher hardness due to the uniform distribution of ZrO_2 nano-particles as well as the refined IMC particles. The hardness values of the plain Sn–Ag–Cu solder joint and solder joints containing 1 wt% of ZrO_2 nano-particles after 5 min reaction at 250 °C were about 15.0 Hv and 17.1 Hv, respectively. On the other hand, their hardness values after 30 min reaction were about 13.7 Hv and 15.5 Hv, respectively.

1. Introduction

Due to the inherent toxicity of lead (Pb) and Pb-containing alloys, environmental regulations and health concerns around the world have been targeted to eliminate the usage of Pb-bearing solders in the electronic packaging industry [1–3]. This has prompted a search for "lead-free" solders and more attention in the research activities in this field. Up to now, several types of binary and ternary Sn-based lead-free solders such as Sn–Ag, Sn–Cu, Sn–Au, Sn–Ag–Cu and Sn–Zn have been developed and applied in the electronic packaging industry [4–6]. Among the various types of lead-free solders, with a combination of process attributes like a modest melting temperature and reasonable solderability, comparable electrical performance and good mechanical properties, Sn–Ag–Cu solder has been proposed as one of the most promising substitutes for conventional Sn–Pb solder [7,8]. Moreover, with the advancement of micro-/nanosystems technology through the years, microelectronic components have evolved to become smaller, lighter and more functional. Therefore, conventional solder technology can on longer guarantee the solder joint reliability of electronic components. In general, the reliability of the solder joints is mainly dependent on an interfacial IMC layer, the difference in coefficients of thermal expansion, the yield strength, elastic modulus, shear strength, fatigue and creep behavior [9]. Studies have revealed that the additions of nano-sized, nonreacting, noncoarsening particles to a solder matrix provide a marked improvement in microstructural modification and mechanical properties [10]. Shen and Chan [11] successfully prepared Sn–9Zn–1 wt% ZrO_2 composite solder by mechanical mixing method, and this composite solder improved the shear strength, suppressed the growth of Sn–Ni IMCs and refined the microstructure. Noh et al. [12] used Ce particles as reinforcements for a conventional Sn–Ag solder and reported significant enhancement in wettability and mechanical properties. Tai et al. [13] prepared 20 vol% Cu_6Sn_5 reinforced Sn–3.5Ag composite solder by an in situ method and the composite solder joint exhibited a better steady-state creep strain rate, less thermomechanical fatigue damage and higher shear strengths after different numbers of thermomechanical fatigue cycles as compared to a plain Sn–3.5Ag solder joint. Xiao et al. [14] reported that rare earth reinforced Sn–Ag–Cu composite solder suppressed the formation of

* Corresponding author. Tel.: +852 27887130; fax: +852 2788 7579.
E-mail address: eeycchan@cityu.edu.hk (Y.C. Chan).

0925-8388/$ – see front matter © 2010 Elsevier B.V. All rights reserved.
doi:10.1016/j.jallcom.2010.12.048

IMCs and refined the microstructure. In addition, the creep-rupture lifetime of the rare earth doped Sn–Ag–Cu solder joint was significantly improved being seven times higher than that of an undoped solder joint. Tsao and Chang [15] found that a Sn–3.8Ag–0.7Cu composite solder reinforced with TiO_2 nano-particles had a significantly improved hardness, yield strength and ultimate tensile strength.

During the reflow process, the formation of IMCs is one of the mechanisms for establishing a strong joint between the liquid solder and substrate. In a Sn–Ag–Cu solder on Cu substrate joint system, a Cu_6Sn_5 IMC layer is formed at the interface. Later, a Cu_3Sn IMC is formed between the Cu and Cu_6Sn_5 by a solid state reaction to satisfy the requirements of local equilibrium [16]. The formation of the IMC layer at the interface is an indication of good bonding between the solder and the metal substrate [17]. However, due to the rapid formation of a brittle Cu_6Sn_5 IMC layer at the Sn-based lead-free solder and Cu substrate interface, the reliability of such solder joints has been a serious concern [18]. It is well known that excessive IMC layer growth affects the mechanical reliability of solder joints [19]. Therefore, to develop reliable lead-free solder joints, it is desirable to understand better the kinetics governing the growth of the interfacial IMCs. The present study investigates the microstructure, hardness and growth kinetics of interfacial IMCs. The aims of this investigation are (1) to determine the interfacial IMCs between Sn–Ag–Cu–1 wt% ZrO_2 solder and OSP-Cu pads, (2) to evaluate the relationship between the growth rate, temperature and time for the formation of IMCs, and (3) to calculate the activation energy of IMCs growth at plain Sn–Ag–Cu and Sn–Ag–Cu–1 wt% ZrO_2 solder/OSP-Cu pads interfaces.

2. Experimental procedures

Composite solders were prepared by mechanically dispersing 1 wt% ZrO_2 nano-particles (Inframat Advanced Materials LLC, USA) into the Sn–3.0Ag–0.5Cu (AMTECH, USA) solder powder. The mixtures were blended manually for at least 30 min to achieve a uniform distribution of ZrO_2 nano-particles with a water-soluble flux (Qualitek Singapore (PTE) Ltd). Then, the paste mixtures were printed on to alumina substrates using a stainless steel stencil with a thickness of 0.15 mm and reflowed in a reflow oven (BTU International, Pyramax-100N) at 250 °C to prepare 0.76 mm diameter solder balls. These, lead-free solder balls were placed on a pre-fluxed OSP-Cu pads and reflowed at various temperatures from 230 to 270 °C with different reaction times in a convection reflow oven (BTU International, Pyramax-100N).

The melting characteristics of plain Sn–Ag–Cu solder and the Sn–Ag–Cu composite solder containing 1 wt% ZrO_2 were investigated using a differential scanning calorimeter (DSC Q 10). For the DSC analysis, 10 mg of each solder was placed into an aluminum pan and scanned from 100 °C to 250 °C at a rate of 10 °C min^{-1} under a nitrogen atmosphere. X-ray diffraction (XRD, Philips PW 3040 X'Pert PRO) was used to determine the crystalline phases of the ZrO_2 nano-particles and the composite solder containing ZrO_2 nano-particles.

To characterize the microstructures, the samples were cross sectioned and mounted in resin, then ground with different grit sized emery papers and polished with a 0.5 μm Al_2O_3 suspension and etched with 5% HCl. Finally, the interfacial morphology at the solder alloy/OSP-Cu substrate interface was observed using a scanning electron microscope (SEM, Philips XL 40 FEG) using the back-scattered electron (BSE) imaging mode and an energy dispersive X-ray spectrometer (EDX, International, model no. DX-4) was utilized to determine the chemical composition of the IMCs. The accuracy of the compositional measurements was typically ±5%. To find out the formula composition of the IMC particles, the chemical analysis of the EDX spectra were corrected by standard atomic number, absorption, fluorescence (ZAF) software [20]. Before SEM observations, the samples were sputter coated with Au to avoid the effects due to charging.

The cross sectioned polished samples were placed in a Vickers hardness tester (FV-700) to measure the microhardness in the solder ball region. The applied load was 0.3 kg for 10 s. The average hardness of fifteen solder balls was taken for each condition.

3. Results and discussion

Fig. 1 shows the differential scanning calorimetry (DSC) results of (a) plain Sn–Ag–Cu solder and (b) solder containing 1 wt% ZrO_2 nano-particles. DSC results showed that the melting point of plain Sn–Ag–Cu solder and solder containing ZrO_2 nano-particles ranged from 217 °C to 217.3 °C with only a eutectic peak. There was an elevation of the melting temperature of less than 1 °C for the ZrO_2 nano-particles containing solder alloy. From these DSC profiles, it was confirmed that it was not required to make any changes to the existing solder process parameters such as the reflow temperature when applying these Sn–Ag–Cu composite solders doped with ZrO_2 nano-particles.

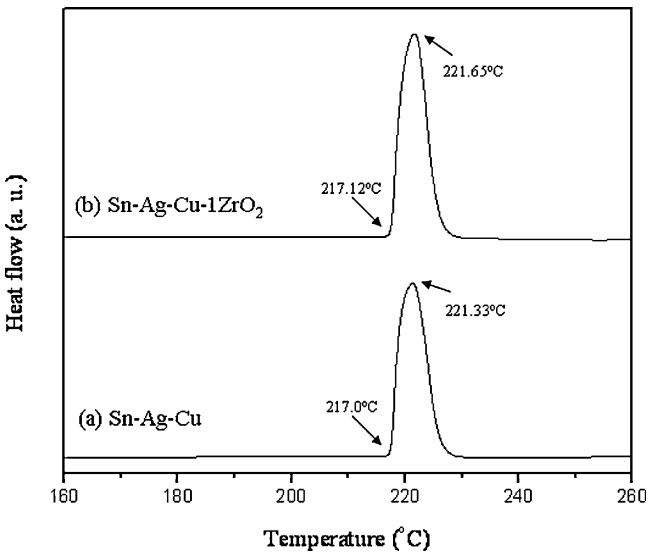

Fig. 1. DSC curves of (a) Sn–Ag–Cu and (b) Sn–Ag–Cu–1 wt% ZrO_2 composite solder alloys.

Fig. 2 shows XRD profiles of (a) ZrO_2 nano-particles and (b) solder alloy containing 1 wt% ZrO_2 nano-particles. In the XRD profile (a), ZrO_2 nano-particles appeared as a crystalline phase with sharp peaks. On the other hand, in the composite solder alloy XRD profile (b), Ag_3Sn, Cu_6Sn_5 IMC particles and the ZrO_2 phase were detected as well as β-Sn phase. It is well know that the dissolved Ag and Cu are precipitated by forming Ag_3Sn and Cu_6Sn_5 IMC particles in the solder matrix during solidification.

Fig. 3 shows backscattered scanning electron micrographs of (a, b) plain Sn–Ag–Cu and (c, d) solder joints containing 1 wt% ZrO_2 nano-particles depending on the reaction time of (a, c) 5 min and

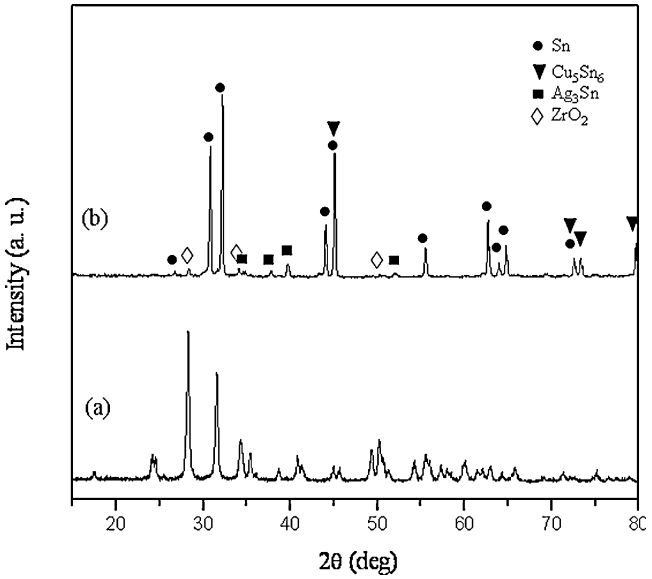

Fig. 2. XRD profiles of (a) ZrO_2 and (b) the Sn–Ag–Cu–1 wt% ZrO_2 composite solder alloy.

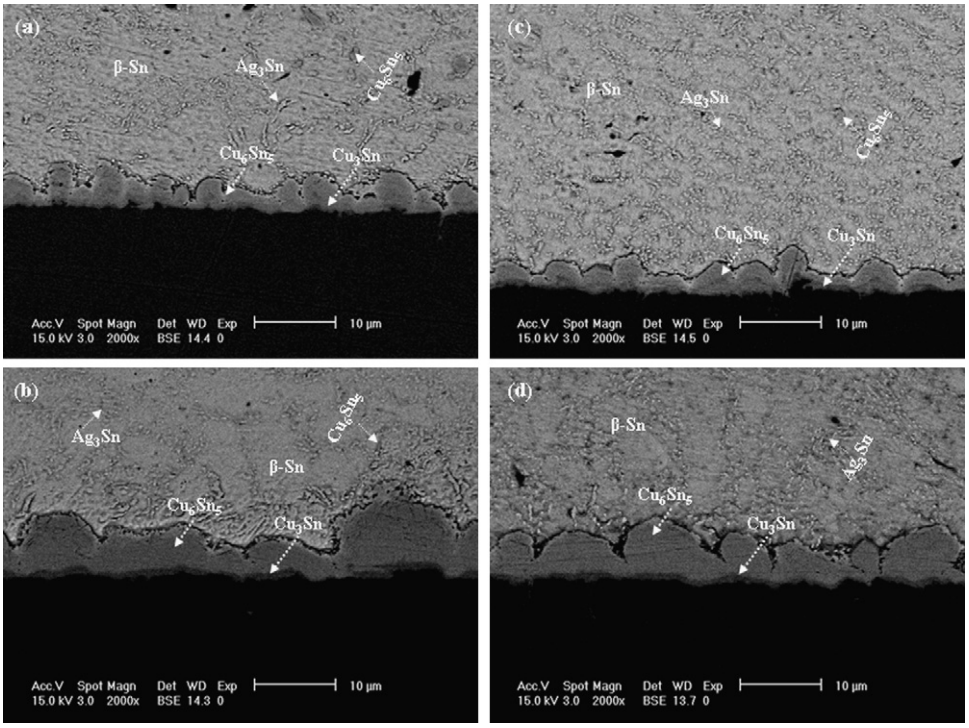

Fig. 3. SEM micrographs of (a, b) Sn–Ag–Cu solder and (c, d) Sn–Ag–Cu–1 wt% ZrO_2 composite solder joints on OSP-Cu pads depending on the reaction time (a, c) 5 min and (b, d) 30 min at 230 °C.

(b, d) 30 min at 230 °C. At their interfaces, an island-shaped Cu_6Sn_5 IMC layer was clearly observed in both solder joints after reaction for 5 min. However, with an increase in the reaction time a scallop-shaped very thin Cu_3Sn IMC with a dark contrast was found between the Cu_6Sn_5 IMC layer and the OSP-Cu pad as indicated in Fig. 3(b) and (d). In addition with an increase in the reaction time the IMC layer thicknesses were significantly increased in both solder joints.

Fig. 4 shows backscattered scanning electron micrographs of (a, b, c) plain Sn–Ag–Cu and (d, e, f) solder joints containing 1 wt% ZrO_2 nano-particles depending on the reaction time of (a, d) 5 min, (b, e) 15 min and (c, f) 30 min at 250 °C. From SEM micrographs, it was clear that the island-shaped Cu_6Sn_5 IMC was found at their interfaces after reaction for 5 min in both solder joints, the same as in Fig. 3. In addition, after a long time reaction a scallop-shaped very thin Cu_3Sn IMC with dark contrast was found between the Cu_6Sn_5 IMC and substrate as shown in Fig. 4(b, c, e, f). In general, the growth of the Cu_3Sn IMC consists of several steps: dissolution of Cu from the OSP-Cu substrate, diffusion of Cu and Sn through the existing Cu_3Sn layer, and conversion of Cu_6Sn_5 into Cu_3Sn at their interfaces and reaction of Sn with Cu at the Cu substrate and Cu_3Sn interface [16,21].

Fig. 5 shows backscattered scanning electron micrographs of (a, b) plain Sn–Ag–Cu and (c, d) solder joints containing 1 wt% ZrO_2 nano-particles depending on the reaction time of (a, c) 5 min and (b, d) 30 min at 250 °C which were taken from the solder ball regions. In the solder ball region, needle-shaped Ag_3Sn and spherically-shaped Cu_6Sn_5 IMC particles were clearly observed in a β–Sn matrix. However, after the addition of ZrO_2 nano-particles, the needle-shaped Ag_3Sn and spherically-shaped Cu_6Sn_5 IMC particles as well as the β-Sn grain size were substantially decreased and appeared with a fine microstructure as shown in Fig. 5(c) and (d). The reason may be that the second phase reinforcement ZrO_2 nano-particles promote a high nucleation density in the eutectic colonies during solidification. Moreover, as effective surface-active materials, ZrO_2 nano-particles will accumulate at the interface of IMC particles. It is well known that the adsorption phenomena plays an important role during solidification process of solder alloys and will greatly affect the microstructure [22]. From this result, it is also clear that the second phase ZrO_2 nano-particles retarded the growth rate of IMC particles and refined the microstructure.

Fig. 6 shows backscattered scanning electron micrographs of (a, b) plain Sn–Ag–Cu and (c, d) solder joints containing 1 wt% ZrO_2 nano-particles depending on the reaction time of (a, c) 5 min and (b, d) 30 min at 270 °C. At their interfaces, an island-shaped Cu_6Sn_5 IMC layer was clearly observed similar to Figs. 4 and 5. From Figs. 4–6, it was clear that with an increase in the reaction temperature the IMC layer thickness was substantially increased. In addition, by increasing the reaction time the island-shaped Cu_6Sn_5 IMC layer thickness was substantially increased in both types of solder joints. However, after the addition of ZrO_2 nano-particles, the island-shaped Cu_6Sn_5 IMC layer growth rate was relatively lower than that in plain Sn–Ag–Cu solder joints. The reason may be that the second phase ZrO_2 nano-particles change the driving force and diffusivity of the IMC layer growth. Li et al. [23] reported that rare earth elements reduce the rate of growth of an IMC layer in two ways, i.e. by altering the diffusion coefficient and the thermodynamic parameters of elemental affinity.

Fig. 7 plots the variation of IMC layer thickness of (a) plain Sn–Ag–Cu solder joints and (b) solder joints containing 1 wt% ZrO_2 nano-particles as a function of the reaction time. The average thickness of the IMC layer was calculated using the following equation: $T = (t_1 + t_2 + t_3 + \ldots + t_n)/n$ where t_1, t_2, t_3,…t_n are the thickness of the IMC layer at various positions at the interface. It may be seen that the IMC layer thickness of all solder joints increased with an increase in the reaction time and temperature. The IMC layer thickness of plain Sn–Ag–Cu solder joints and solder joints containing 1 wt% ZrO_2 nano-particles after 5 min reaction at 250 °C were about 3.51 μm and 3.41 μm, respectively while their IMC thickness after 30 min reaction were about 7.82 μm and 6.81 μm, respectively.

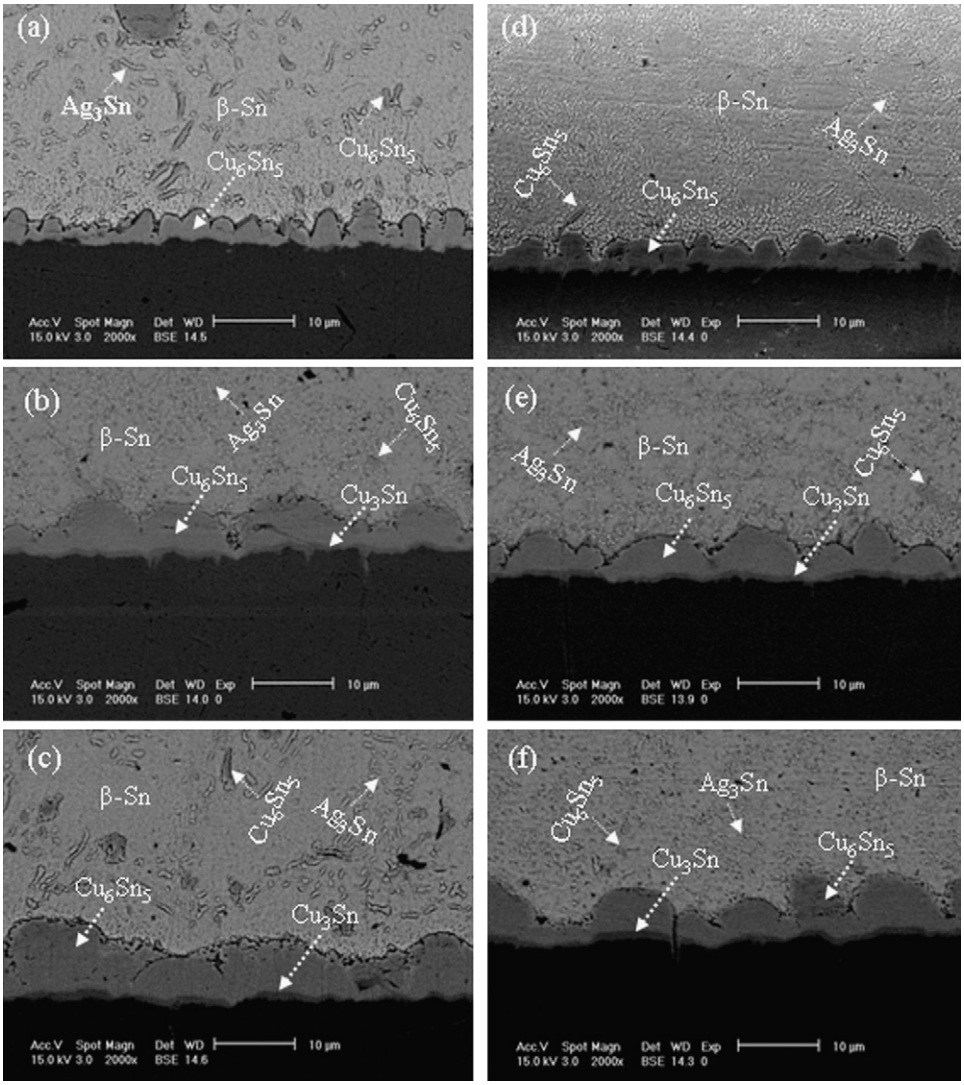

Fig. 4. SEM micrographs of (a, b, c) Sn–Ag–Cu solder and (d, e, f) Sn–Ag–Cu–1 wt% ZrO_2 composite solder joints on OSP-Cu pads depending on the reaction time (a, d) 5 min, (b, e) 15 min and (c, f) 30 min at 250 °C.

From this result, it is clear that the ZrO_2 nano-particles retarded the growth of the IMC layer.

Fig. 8 gives plots of the square IMC layer thickness versus reaction time at various temperatures. Each plot displays a linear relationship, so it can be assumed the growth of IMC layer is controlled by a diffusion process [24]. Generally, the thickness of an interfacial reaction layer has been modeled as a diffusion driven process which can be expressed by $d = kt^n$, where d is the thickness of the IMC layer during reflow; k is the growth rate constant; n is the time exponent; and t is the interfacial reaction time. The growth rate constant was calculated from the slope of the line for each temperature in both solder joints.

To obtain the activation energy of IMC growth at the solder alloy and OSP-Cu interface, the temperature variations of growth rate constant k can be expressed by an Arrhenius equation in terms of an interdiffusion coefficient: $k = k_o \exp(-Q/RT)$, where k_o is the interdiffusion constant; Q is activation energy for growth of the interfacial IMC layer; R is the gas constant ($R = 8.314$ kJ/mol); and T is the absolute temperature. Fig. 9 shows plots of lnk versus $1/T$ of plain Sn–Ag–Cu solder joints and solder joints containing 1 wt% ZrO_2 nano-particles. The value of the activation energies for the total ($Cu_6Sn_5 + Cu_3Sn$) IMC layers for plain Sn–Ag–Cu solder joints and solder joints containing 1 wt% ZrO_2 nano-particles on OSP-Cu pads were about 53.2 and 59.5 kJ/mol, respectively. Consequently, the intermetallic growth rate is higher for Sn–Ag–Cu/OSP-Cu system than for the Sn–Ag–Cu–1ZrO_2/OSP-Cu system according to the smaller activation energy for the growth of total ($Cu_6Sn_5 + Cu_3Sn$) IMC layers. The extent of IMC growth depends on the thermal conditions and the integrity of the solder joints is influenced by the properties of the IMC layers [25].

The measurement of hardness, especially microhardness, is the usual method to characterize the mechanical properties of materials. The hardness of a material is often equated with its resistance to wear and is a characteristic of practical interest since it determines the durability of a material during use and it also decides the suitability of the material for particular applications. Microhardness tests are made to determine the hardness of total grains, phases and structural components of alloys. The microhardness of a solder alloy depends on the motion of dislocations and growth and configuration of grains. These processes are more sensitive to the microstructure, temperature and composition. Fig. 10 shows microhardness values of the plain Sn–Ag–Cu solder joints and solder joints containing 1 wt% ZrO_2 nano-particles as a function of reaction time between the molten solders and OSP-Cu pads at

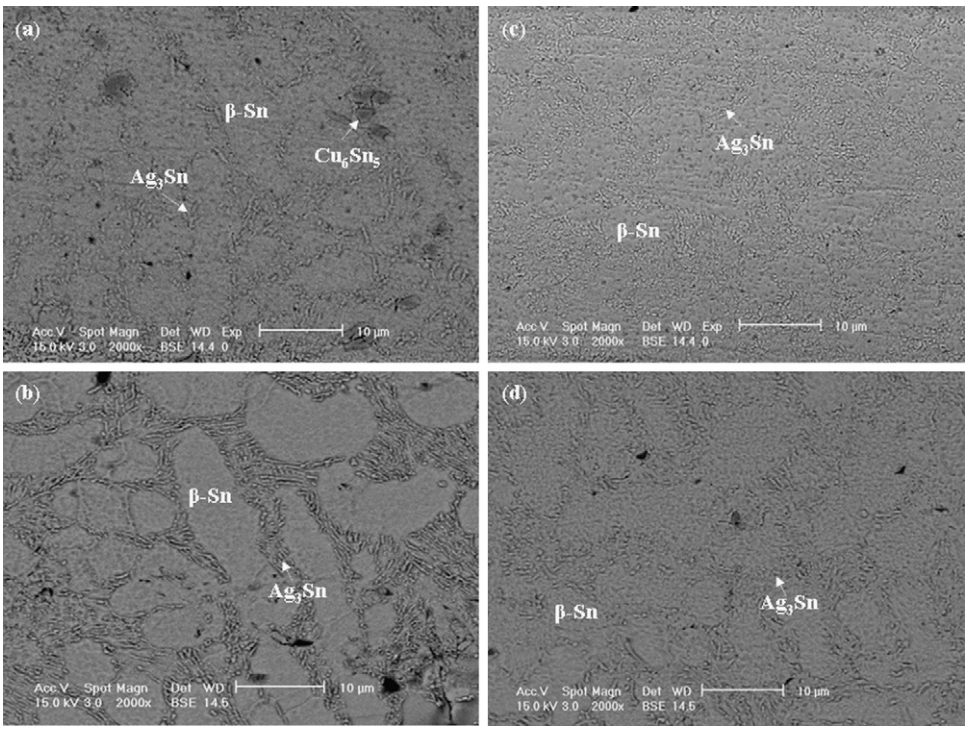

Fig. 5. SEM micrographs of (a, b) Sn–Ag–Cu solder and (c, d) Sn–Ag–Cu–1 wt% ZrO_2 composite solder joints on OSP-Cu pads depending on the reaction time (a, c) 5 min and (b, d) 30 min at 250 °C.

250 °C. The hardness of solder joints containing ZrO_2 nano-particles displayed a consistently higher value than those of the plain solder joints due to the homogeneous distribution of ZrO_2 nano-particles and the refined IMC particles, i.e. Ag_3Sn, Cu_6Sn_5 which can act as reinforcement phases. According to dispersion strengthening mechanisms, the fine IMC particles and ZrO_2 nano-particles can improve the mechanical properties of a solder joint. This can be attributed to (1) pinning of grain boundaries, (2) obstacles to the movement of dislocations and increasing the dislocation densities and (3) a strengthening mechanism of the matrix, finely dispersed

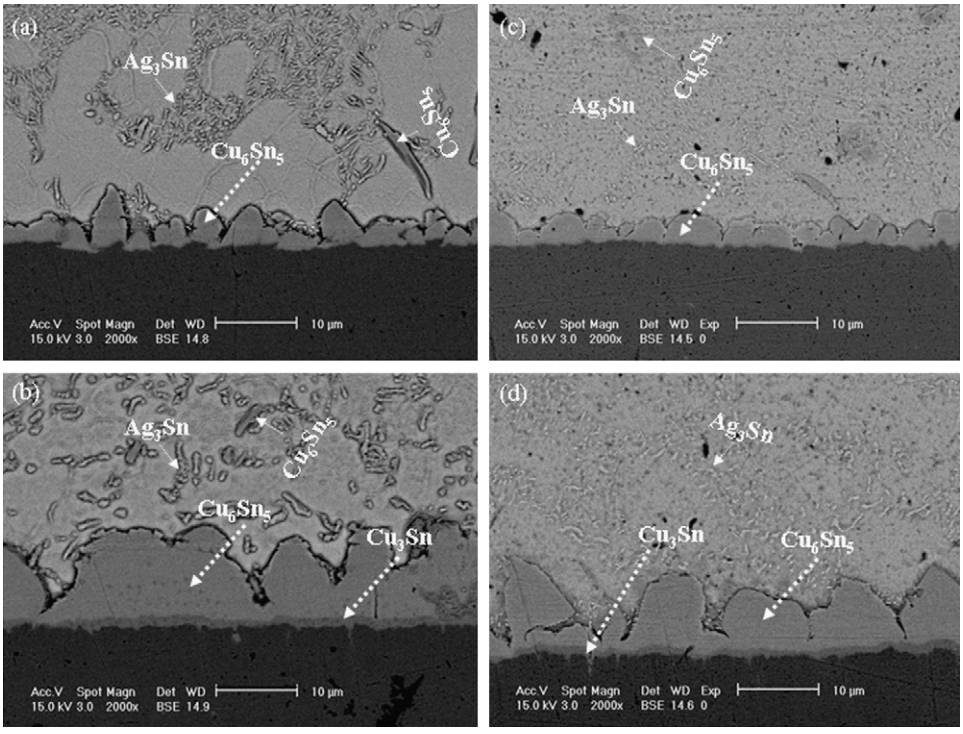

Fig. 6. SEM micrographs of (a, b) Sn–Ag–Cu solder and (c, d) Sn–Ag–Cu–1 wt% ZrO_2 composite solder joints on OSP-Cu pads depending on the reaction time (a, c) 5 min and (b, d) 30 min at 270 °C.

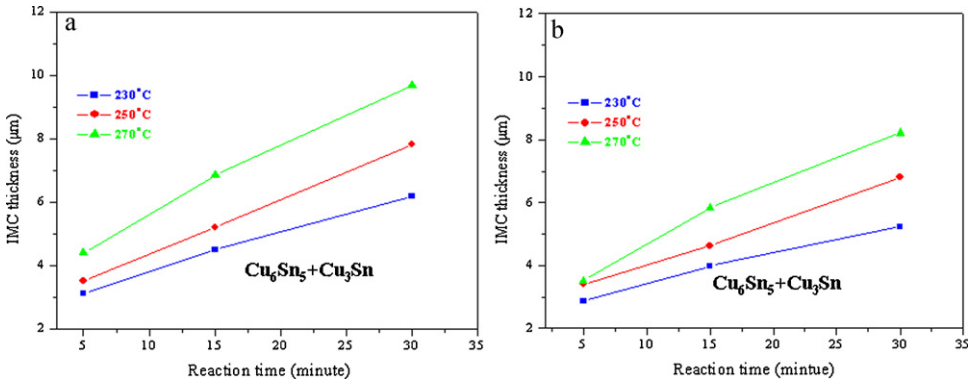

Fig. 7. Thickness (d) of Cu intermetallic compounds as a function of reaction time between liquid (a) Sn–Ag–Cu and (b) Sn–Ag–Cu–1 wt% ZrO_2 composite solder/OSP-Cu pad substrates at various temperatures.

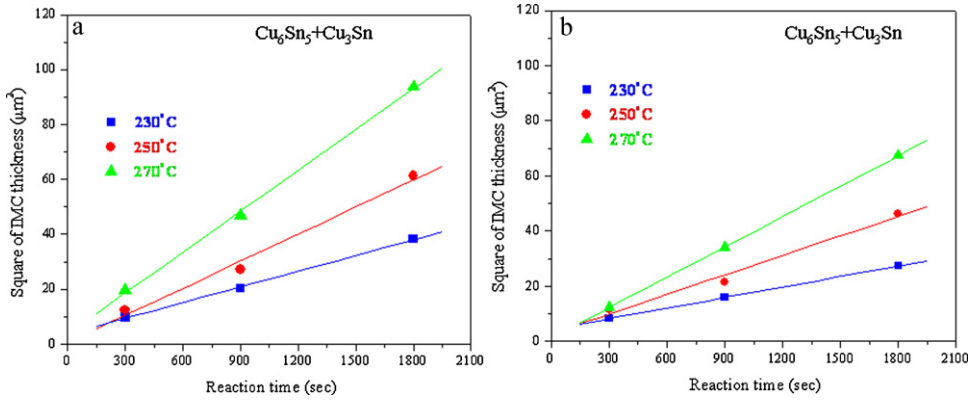

Fig. 8. Thickness (d^2) of Cu intermetallic compounds as a function of reaction time between liquid (a) Sn–Ag–Cu and (b) Sn–Ag–Cu–1 wt% ZrO_2 composite solder/OSP-Cu pad substrates at various temperatures.

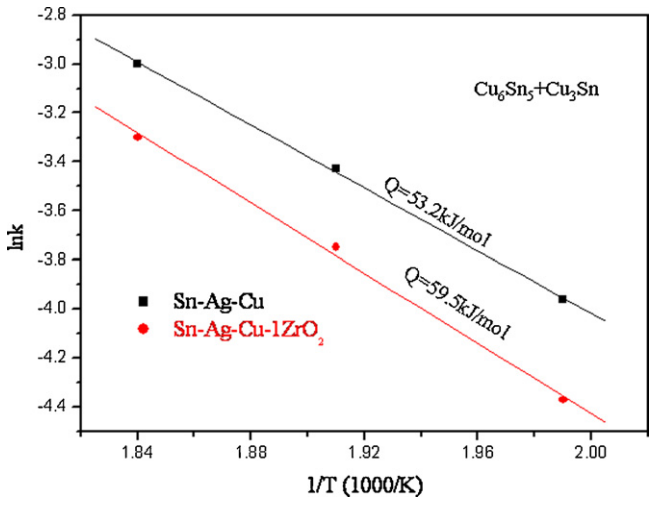

Fig. 9. Arrhenius plots for the IMC growth in Sn–Ag–Cu solder and Sn–Ag–Cu–1 wt% ZrO_2 composite solder/OSP-Cu pad substrates interfacial reactions.

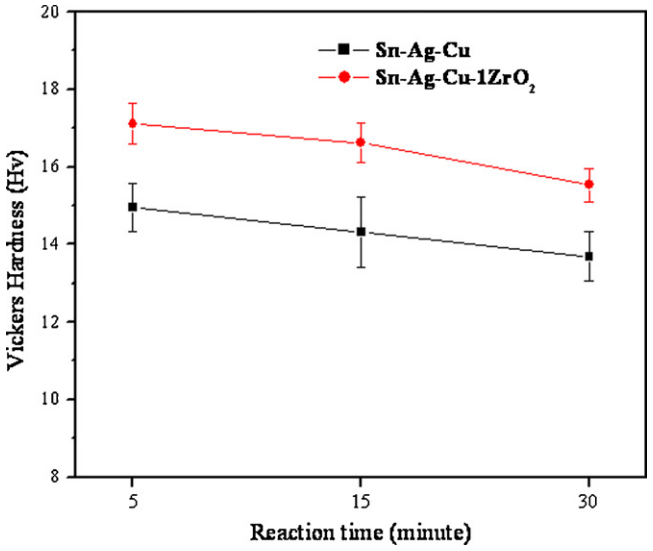

Fig. 10. Hardness of plain Sn–Ag–Cu and Sn–Ag–Cu–1 wt% ZrO_2 solder joints as a function of the reaction time at 250 °C.

IMC particles and ZrO_2 nano-particles [26]. The microhardness values of the plain Sn–Ag–Cu solder joints and solder joints containing 1 wt% of ZrO_2 nano-particles after 5 min reaction at 250 °C were about 15.0 Hv and 17.1 Hv, respectively. On the other hand, their microhardness values after 30 min reaction at 250 °C were about 13.7 Hv and 15.5 Hv, respectively.

4. Conclusions

The liquid-state interfacial reactions between plain Sn–Ag–Cu solder joints and solder joints containing ZrO_2 nano-particles with OSP-Cu pads were investigated as a function of reaction time at various temperatures. After the reflow at various tem-

peratures and different reaction times, an island-shaped Cu_6Sn_5 and Cu_3Sn IMC layers were formed at their interfaces and the IMC layers thicknesses were substantially increased with an increase in the temperature and reaction time. In the solder ball region, needle-shaped Ag_3Sn and spherically-shaped Cu_6Sn_5 IMC particles were found to be homogeneously distributed in the β–Sn matrix. However, after the addition of ZrO_2 nano-particles, needle-shaped Ag_3Sn and spherically-shaped Cu_6Sn_5 IMC particles appeared with a fine microstructure and also suppressed the formation of IMC layers. From a kinetic analysis, the calculated activation energies for the total ($Cu_6Sn_5 + Cu_3Sn$) IMC layers for Sn–Ag–Cu and Sn–Ag–Cu–1 wt% ZrO_2 composite solder joints on OSP-Cu pads were about 53.2 and 59.5 kJ/mol, respectively.

The solder joints containing 1 wt% ZrO_2 nano-particles showed a consistently higher hardness than that of the plain solder joints. It is reasonable to suggest that the hardness of the bulk solder was enhanced by the addition ZrO_2 nano-particles because the ZrO_2 nano-particles dispersion strengthened the solder as well as refining the microstructure.

Acknowledgements

The authors acknowledge the financial support provided by City University of Hong Kong for the project 9041222 CERG grant of Hong Kong Research Grants Council and RGC ref. no. 111307 (Development of a nano-activator doped surface modifier for Sn–Zn based lead-free soldering). Professor Brian Ralph is thanked for proof reading the manuscript.

References

[1] S.E. Negm, H. Mady, A.A. Bahgat, J. Alloys Compd. 503 (2010) 65–70.
[2] L. Liu, W. Zhou, B. Li, P. Wu, J. Alloys Compd. 482 (2009) 90–98.
[3] A.K. Gain, Y.C. Chan, A. Sharif, W.K.C. Yung, Microelectron. Eng. 86 (2009) 2347–2353.
[4] S.H. Wang, T.S. Chin, C.F. Yang, S.W. Chen, C.T. Chuang, J. Alloys Compd. 497 (2010) 428–431.
[5] C.Y. Lin, U.S. Mohanty, J.H. Chou, J. Alloys Compd. 501 (2010) 204–210.
[6] R.M. Shalaby, J. Alloys Compd. 505 (2010) 113–117.
[7] C. Han, Q. Liu, D.G. Ivey, Mater. Sci. Eng. B 164 (2009) 172–179.
[8] W. Tang, H. Zang, Y. Wu, Z. Zheng, J. Alloys Compd. 497 (2010) 396–401.
[9] J. Shen, Y.C. Chan, J. Alloys Compd. 477 (2009) 909–914.
[10] T. Fouzder, A.K. Gain, Y.C. Chan, A. Sharif, N.B. Wong, W.K.C. Yung, Microelectron. Reliab. 50 (2010) 2051–2058.
[11] J. Shen, Y.C. Chan, J. Alloys Compd. 477 (2009) 552–559.
[12] B.I. Noh, J.H. Choi, J.W. Yoon, S.B. Jung, J. Alloys Compd. 499 (2010) 154–159.
[13] F. Tai, F. Guo, M.T. Han, Z.D. Xia, Y.P. Lei, Y.W. Shi, Mater. Sci. Eng. A 527 (2010) 3335–3342.
[14] W.M. Xiao, Y.W. Shi, G.C. Xu, R. Ren, F. Guo, Z.D. Xia, Y.P. Lei, J. Alloys Compd. 472 (2009) 198–202.
[15] L.C. Tsao, S.Y. Chang, Mater. Des. 31 (2010) 990–993.
[16] C.C. Chang, Y.W. Lin, Y.W. Wang, C.R. Kao, J. Alloys Compd. 492 (2010) 99–104.
[17] M.H. Tsai, W.M. Chen, M.Y. Tsai, C.R. Kao, J. Alloys Compd. 504 (2010) 341–344.
[18] F. Cheng, F. Gao, H. Nishikawa, T. Takemoto, J. Alloys Compd. 472 (2009) 530–534.
[19] P. Liu, p. Yao, J. Liu, J. Alloys Compd. 486 (2009) 474–479.
[20] J.I. Goldstein, D.E. Newbury, P. Echlin, D.C. Joy, A.D. Romig Jr., C.E. Lyman, C. Fiori, E. Lifshin, Scanning Electron Microscopy and X-ray Microanalysis, 2nd ed., Plenum, New York, 1992.
[21] J.W. Yoon, B.I. Noh, B.K. Kim, C.C. Shur, S.B. Jung, J. Alloys Compd. 486 (2009) 142–147.
[22] L.C. Tsao, J. Alloys Compd. (2010), doi:10.1016/j.jallcom.2010.11.010.
[23] B. Li, Y.W. Shi, Y.P. Lei, F. Guo, Z.D. Xia, B. Zong, J. Electron. Mater. 34 (3) (2005) 217–224.
[24] A. Sharif, Y.C. Chan, M.N. Islam, M.J. Rizvi, J. Alloys Compd. 388 (2005) 75–82.
[25] M.C. Wang, S.P. Yu, T.C. Chang, M.H. Hon, J. Alloys Compd. 381 (2004) 162–167.
[26] Y. Shi, J. Liu, Z. Xia, Y. Lei, F. Guo, X. Li, J. Mater. Sci. Mater. Electron. 19 (2008) 349–356.